Article

A Chemomechanical Model of Matrix and Nuclear Rigidity Regulation of Focal Adhesion Size

Xuan Cao,[1] Yuan Lin,[2] Tristian P. Driscoll,[3] Janusz Franco-Barraza,[4] Edna Cukierman,[4] Robert L. Mauck,[3,5] and Vivek B. Shenoy[1,5,*]

[1]Department of Materials Science and Engineering, School of Engineering and Applied Science, The University of Pennsylvania, Philadelphia, Pennsylvania; [2]Department of Mechanical Engineering, The University of Hong Kong, Hong Kong SAR, China; [3]Department of Orthopaedic Surgery, Perelman School of Medicine, University of Pennsylvania, Philadelphia, Pennsylvania; [4]Cancer Biology Program, Fox Chase Cancer Center, Temple Health, Philadelphia, Pennsylvania; and [5]Department of Bioengineering, School of Engineering and Applied Science, University of Pennsylvania, Philadelphia, Pennsylvania

ABSTRACT In this work, a chemomechanical model describing the growth dynamics of cell-matrix adhesion structures (i.e., focal adhesions (FAs)) is developed. We show that there are three regimes for FA evolution depending on their size. Specifically, nascent adhesions with initial lengths below a critical value that are yet to engage in actin fibers will dissolve, whereas bigger ones will grow into mature FAs with a steady state size. In adhesions where growth surpasses the steady state size, disassembly will occur until their sizes are reduced to the equilibrium state. This finding arises from the fact that polymerization of adhesion proteins is force-dependent. Under actomyosin contraction, individual integrin bonds within small FAs (i.e., nascent adhesions or focal complexes) must transmit higher loads while the phenomenon of stress concentration occurs at the edge of large adhesion patches. As such, an effective stiffness of the FA-extracellular matrix complex that is either too small or too large will be relatively low, resulting in a limited actomyosin pulling force developed at the edge that is insufficient to prevent disassembly. Furthermore, it is found that a stiffer extracellular matrix and/or nucleus, as well as a stronger chemomechanical feedback, will induce larger adhesions along with a higher level of contraction force. Interestingly, switching the extracellular side from an elastic half-space, corresponding to some widely used in vitro gel substrates, to a one-dimensional fiber (as in the case of cells anchoring to a fibrous scaffold in vivo) does not qualitative change these conclusions. Our model predictions are in good agreement with a variety of experimental observations obtained in this study as well as those reported in the literature. Furthermore, this new model, to our knowledge, provides a framework with which to understand how both intracellular and extracellular perturbations lead to changes in adhesion structure number and size.

INTRODUCTION

To perform functions such as proliferation (1), differentiation (2), and locomotion (3), living cells establish stable attachments to the extracellular matrix (ECM) via the formation of specialized receptor-mediated contact foci. Among all adhesion structures perhaps the best-known are focal adhesions (FAs), with a molecular structure composed of a diverse population of structural and signaling proteins. Roughly speaking, individual integrin receptors, responsible for forming molecular bonds between ECM ligands and intracellular adhesion proteins, are laterally reinforced by a layer/complex of proteins including vinculin, paxillin, and talin (4), collectively known as the adhesome or adhesion patch. This layer of proteins is then connected to the cytoskeleton/nucleus of the cell via stress fibers, composed of actin filaments and myosin motors. In addition to physically linking the cytoskeleton to the ECM, FAs also serve as signaling hubs for cells to receive information from their microenvironment and hence are believed to play key roles in processes such as development (5,6), tumorigenesis (7,8), and wound healing (9).

Interestingly, besides biochemical factors, accumulating evidence has demonstrated that formation and function of FAs is tightly regulated by mechanical cues (10–16). For example, it has been shown that forces generated by actomyosin contraction are essential for the stabilization of FAs (10). Furthermore, FAs display directional growth parallel to an externally applied load (11). Numerous observations also indicate that cells form larger (and more) FAs on stiffer substrates as well as develop higher intracellular traction forces (12–16). Various attempts have been made to theoretically explain the force-induced growth of FAs via thermodynamic arguments (17) or by examining the anisotropic stress/strain field generated in the adhesion plaque (18,19). The lifetime/stability of adhesion structures (i.e., clusters) has also been analyzed by considering the nonuniform load distribution among molecular bonds as well as their force-modulated association/dissociation kinetics (20–22). Recently, the question of how ECM rigidity affects integrin dynamics in cells has been examined by several studies that suggest that a compliant substrate will generally

Submitted March 16, 2015, and accepted for publication August 31, 2015.

*Correspondence: vshenoy@seas.upenn.edu

Editor: Sean Sun.

0006-3495/15/11/1807/11

http://dx.doi.org/10.1016/j.bpj.2015.08.048

impair integrin clustering (23,24) and lead to oscillatory traction forces along with a slow retrograde flow of F-actin (25,26).

Despite these aforementioned efforts, several important issues remain unsettled. First, in most existing models, the size of the adhesion plaque is often taken as a constant (18–22) or is not included in the formulation (25,26). Likewise, ECM rigidity is often not taken into consideration in some models (17). In reality, it is conceivable that small adhesion patches can be nucleated and, depending on factors like its initial size and the stimuli received, a nascent structure (i.e., focal complex) can either grow into a mature adhesion (i.e., FA) or totally dissolve (27,28). Significant efforts have been made to model the formation and evolution of FAs. For instance, by describing various processes involved in FA assembly via rate equations, a theoretical model (29) has been developed that captures several experimental findings. However, determining different rate parameters from experiments remains challenging. Recently, a stochastic model was also proposed by considering the force-dependent integrin binding/unbinding that drives FA growth/decay (30). This description successfully predicts sizes of FAs that were comparable to experimental observations. One assumption in this model is that the force acting on each integrin was assumed to be the same and along the normal direction. However, recent observations have indicated that the force distribution within a FA is nonuniform (12) and that the majority of force is actually applied tangentially to FAs (31). Given that the size of FAs is believed to significantly affect processes like cell migration (32) and actin recruitment/polymerization (33), this issue should be of great fundamental and practical interest. In addition, the question of whether (and how) cells will anchor themselves differently on a flat surface, like synthetic gel substrates with low porosity, or in a fibrous in-vivo-like scaffold has attracted increasing attention experimentally (34,35). However, it seems that very few modeling efforts have been spent to address this important issue. Finally, recent observations also suggested that the physical properties of cell nucleus (12,13) can influence the size of adhesion plaques (i.e., FAs) and intracellular tension levels, but, to the best of our knowledge, no theoretical explanation has been provided.

To address these concepts, we developed a chemomechanical model to describe the growth dynamics of adhesion plaques where important features such as the actomyosin feedback and nucleus deformability have all been taken into account. In particular, we show that pulling forces large enough to induce further assembly of adhesion proteins can only be developed at the edge of a plaque when its size is within an intermediate range, reflecting the fact that integrin bonds within small/nascent focal complexes must transmit higher loads while the phenomenon of stress concentration will take place at the edge of large adhesion patches (i.e., stabilizing as FAs). In addition, the model predicts that both nuclear and ECM rigidities tightly regulate the equilibrium length of fully developed FAs, with a stiffer surrounding environment or nucleus leading to larger adhesion plaques coupled with a higher intracellular traction force. Interestingly, switching the extracellular side from an elastic half-space (i.e., as many in vitro substrate/gels) to a one-dimensional fiber (simulating in vivo mesenchymal fibrous microenvironments) does not lead to qualitative changes to these conclusions. Connections between our model predictions and various experimental observations will also be discussed.

MATERIALS AND METHODS

Model formulation: mechanical response of the system

In light of the fact that a focal adhesion (consisting of individual integrins that bind to the ECM and to an intracellular layer/complex of reinforcing actin binding proteins) is connected to the cell nucleus via the actomyosin stress fiber (Fig. 1 *a*), a structural model as shown in Fig. 1 *b* is adopted here to describe the response of this ECM/FA (including adaptor adhesome proteins)-actomyosin-nucleus assembly. For simplicity, the FA-ECM complex is treated as a spring (*green box* in Fig. 1 *b*) with effective stiffness depending on the FA size and mechanical properties of the ECM, as will be illustrated later. In addition, a contractile element in parallel with a linear spring (*blue box* in Fig. 1 *b*) is used to represent myosin motors in the elastic actin stress fibers. Finally, the cell nucleus is modeled as another spring to reflect its deformability.

At this point, it is necessary to differentiate two types of extracellular environments that a cell can sense (on its ventral side). For the case of cells anchoring themselves in a scaffold composed of fibers, such as collagen fibrils with diameters on the order of hundreds of nanometers (36,37) that are comparable to the size of FAs, it is reasonable to treat the ECM as an elastic fiber (Fig. 1 *c*), given that the entire adhesion structure (i.e., three-dimensional matrix adhesion) will likely be formed on a single fiber (38). On the other hand, for many synthetic substrates (such as PDMS and PAA) with low porosity, the anchoring distance between ECM proteins coated on the surface to induce formation of cell-ECM adhesion is generally small. In this case, the cell may not see the ventral side as an individual fiber, but rather as a continuous medium (Fig. 1 *d*). We proceed by considering both of these cases in this study.

If the adhesion plaque is treated as an elastic fiber of length, L, connected to the ECM via a series of equally spaced springs representing the integrin bonds formed, then the force generated in the substrate (γ_s) and the plaque (γ_p) can be expressed as $\gamma_s = k_s d_c du_s/dx$ and $\gamma_p = k_p d_c du_p/dx$, respectively, where k_s and u_s (or k_p and u_p) are, respectively, the stiffness and displacement of the ECM (or the adhesion plaque), and d_c is the spacing between integrins. Equilibrium requires that γ_s and γ_p must be related to the integrin clutch force γ_c through

$$d_c \frac{d\gamma_p(x)}{dx} = -d_c \frac{d\gamma_s(x)}{dx} = \gamma_c(x). \tag{1}$$

Because each integrin bond is modeled as a spring, γ_c takes the simple form

$$\gamma_c(x) = k_c\big(u_p(x) - u_s(x)\big), \tag{2}$$

where k_c is the effective spring constant of the clutch. Note that possible sliding-induced friction between the adhesion plaque and the ECM has been neglected here for simplicity. It was widely reported that integrin binding can occur within seconds (12,25,26), which is much faster than the

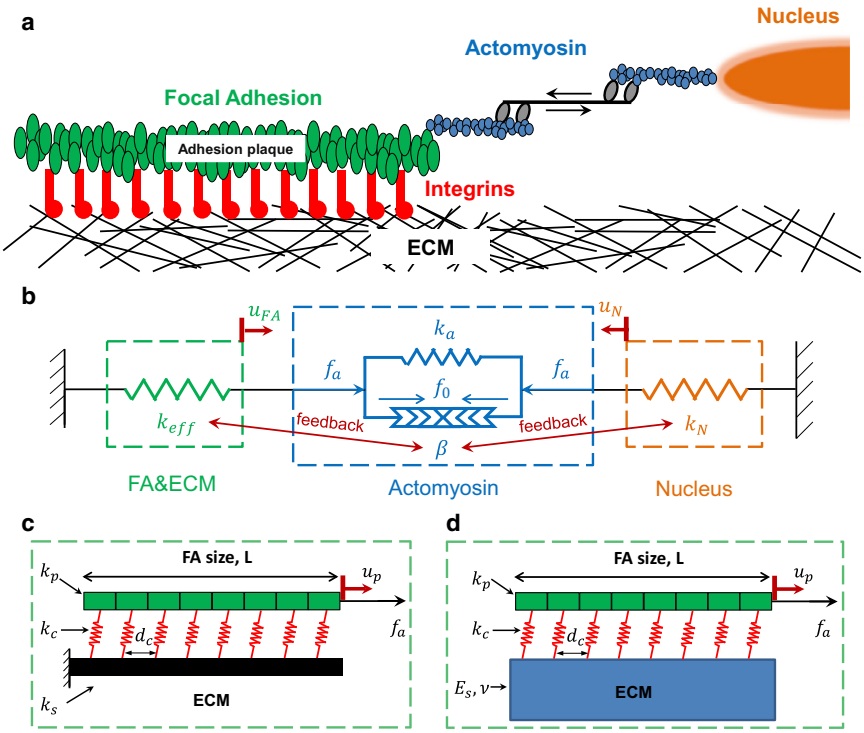

FIGURE 1 (*a*) Schematic representation of the cell-to-ECM adhesions. (*b*) Structural model of the ECM/FA-Actomyosin-Nucleus assembly. Two types of ECM are considered in this study: a one-dimensional elastic fiber (*c*) and a continuous elastic medium (*d*), in which d_c indicates integrin spacing and adhesion plaque is assumed to consist of the units of plaque protein complex (*green block*) and integrin (*red spring*). To see this figure in color, go online.

assembly of proteins in the FA (taking minutes to complete (39)). Therefore, in this study, it is assumed that assembly of the adhesion plaque is the rate-limiting step and that new integrin bonds will be rapidly formed as the adhesion plaque grows. On the other hand, once formed, the integrin-ECM bonds are treated as permanent unless disassembly of plaque proteins takes place at the corresponding site for the given time frame. With the help of Eq. 2, Eq. 1 can finally be simplified to

$$\begin{cases} k_p d_c^2 \dfrac{d^2 u_p}{dx^2} = k_c(u_p - u_s), \\ k_s d_c^2 \dfrac{d^2 u_s}{dx^2} = -k_c(u_p - u_s). \end{cases} \tag{3}$$

We proceed by assuming that the ECM is fixed at one end and free at the other, i.e., $u_s(0) = 0$ and $du_s/dx|_{x=L} = 0$ (refer to Fig. 1 *c*), while the plaque is pulled by the actomyosin force f_a on the side proximal and remains traction-free at the other, i.e., $k_p d_c du_p/dx|_{x=L} = f_a$ and $du_p/dx|_{x=0} = 0$ (refer to the Supporting Material for a detailed discussion on the boundary conditions). To make sure that there is room for integrins to bind, the ECM fiber beneath the FA is assumed to be of the same size as the FA. Solutions of Eq. 3, satisfying all the imposed boundary conditions, can be obtained as

where L_c is a characteristic length defined by

$$L_c = d_c \sqrt{\frac{k_p k_s}{k_c(k_p + k_s)}}. \tag{5}$$

$4L_c$ gives a length-scale far below which force is more or less evenly shared by the integrins within the plaque, while beyond this length the load will only be transmitted to integrin bonds within a distance ~$2L_c$ from the adhesion edge.

Given that the pulling force f_a is acting at the end of the adhesion plaque, the effective stiffness of the FA/ECM complex can be defined as

$$k_{\text{eff}} = f_a / u_{FA}, \tag{6}$$

with u_{FA} being the displacement of the plaque at $x = L$, that is,

$$u_{FA} = u_p(x = L) = \frac{f_a L_c}{d_c(k_p + k_s)} \left[\frac{L}{L_c} + 2\operatorname{csch}\left(\frac{L}{L_c}\right) + \left(\frac{k_p}{k_s} + \frac{k_s}{k_p}\right) \coth\left(\frac{L}{L_c}\right) \right]. \tag{7}$$

$$\begin{cases} u_p(x) = \dfrac{f_a L_c}{d_c k_p (k_p + k_s)} \left[k_p \dfrac{x}{L_c} + \operatorname{csch}\left(\dfrac{L}{L_c}\right) \left(k_p \cosh\left(\dfrac{L - x}{L_c}\right) + k_s \cosh\left(\dfrac{x}{L_c}\right) \right) \right] + \dfrac{f_a L_c}{d_c k_s (k_p + k_s)} \left(k_p \coth\left(\dfrac{L}{L_c}\right) + k_s \operatorname{csch}\left(\dfrac{L}{L_c}\right) \right), \\ u_s(x) = \dfrac{f_a L_c}{d_c k_s (k_p + k_s)} \left[k_s \dfrac{x}{L_c} - \operatorname{csch}\left(\dfrac{L}{L_c}\right) \left(k_p \cosh\left(\dfrac{L - x}{L_c}\right) + k_s \cosh\left(\dfrac{x}{L_c}\right) \right) \right] + \dfrac{f_a L_c}{d_c k_s (k_p + k_s)} \left(k_p \coth\left(\dfrac{L}{L_c}\right) + k_s \operatorname{csch}\left(\dfrac{L}{L_c}\right) \right), \end{cases} \tag{4}$$

If, on the other hand, the ECM is treated as a continuous medium (Fig. 1 *d*), then the Green's function for an elastic half-plane (40) can be used to relate the integrin clutch force to the substrate displacement (refer to the Supporting Material). The governing equations in this case become

$$\begin{cases} k_p d_c^2 \dfrac{d^2 u_p}{dx^2} = k_c\left(u_p - u_s\right) \\ u_s(x) = \displaystyle\int_0^L \frac{1+\nu}{\pi E_s}\frac{1}{|x-t|} k_c\left[u_p(t) - u_s(t)\right] dt, \end{cases} \tag{8}$$

where E_s and ν, respectively, are the elastic modulus and Poisson's ratio (taken to be 0.5 because most biological materials are known to be incompressible) of the ECM. Because closed-form solutions for the elastic fields cannot be derived in this case, numerical techniques are employed to obtain the relationship between f_a (i.e., the pulling force acting on FA) and u_{FA} (i.e., the substrate displacement at the location where the force is applied). This allows us to estimate the apparent stiffness of the FA, k_{eff}, defined in Eq. 6. Specifically, in this study, numerical simulations were carried out using the finite-element package COMSOL (COMSOL, Burlington, MA) where an elastic fiber (representing the adhesion plaque) was pulled at one end on a large elastic substrate, with springs connecting them (refer to the Supporting Material for details).

Finally, to determine the magnitude of f_a, recall that the actomyosin network is represented by a contractile element in parallel with a linear spring (Fig. 1 *b*). Using mechanical force balance shown in Fig. 1 *b*, we have

$$f_a = f_0 - k_a(u_{FA} - u_N) + \beta f_a, \tag{9}$$

where k_a represents the stiffness of stress fiber, f_0 stands for the base level contractile force generated by myosin motors, and β stands for the chemomechanical feedback effect. Base-level contractile force is defined as the total force generated by motors associated with one FA without activation of force-dependent stress fiber/myosin motor recruitment. For simplicity, the FA is assumed to be static on the ECM, and therefore the myosin motors are in a stall state (sliding velocity is zero) and f_0 represents the stall force. Stresses on FAs activate signaling pathways that initiate active myosin motors and stress fiber recruitment (41,42). Recruited myosin motors and stress fibers will in return further enhance the forces acting on FAs, thus forming a chemomechanical feedback system. The feedback parameter β is introduced to capture the essential effect in the system, which is to increase the contractile force over the baseline value. For simplicity, this parameter is taken as a constant (0.8) in the allowable range of 0 to1. Because the nucleus is simplified as a spring (with a spring constant k_N), its displacement under actomyosin contraction is

$$u_N = -\frac{f_a}{k_N}. \tag{10}$$

Combining Eqs. 6, 9, and 10, the pulling force generated by actomyosin can be obtained as

$$f_a = \frac{f_0}{1 - \beta + \left[\frac{k_a}{k_{\mathrm{eff}}} + \frac{k_a}{k_N}\right]}. \tag{11}$$

Note that the pulling force increases with increasing feedback parameter and with increasing nuclear stiffness and the effective stiffness of the adhesion plaque, which in turn depends on its length and the stiffness of the ECM.

Model formulation: growth dynamics of the adhesion plaque

With the elastic fields within the FA at hand, we can now consider its growth via recruitment of additional adhesion proteins (e.g., vinculin, talin, paxillin) into the plaque. To simplify the analysis, we proceed by assuming that protein recruitment/disassembly can only take place at the ends of the plaque as suggested in other models (18) and progresses in a quasi-equilibrium manner. In addition, we express the chemical potential difference of a segment of protein (with length d_c) assembled into the plaque and in the cytosol as

$$\Delta\mu = 2\Delta\mu_0 + \Delta E_{re}, \tag{12}$$

where $\Delta\mu_0$ is the chemical potential change in the absence of mechanical load (the factor 2 comes from the fact that the plaque can grow at either end), and ΔE_{re} is the mechanical contribution (17), which takes the form

$$\Delta E_{re} = -f_a d_c, \tag{13}$$

consistent with experimental observations (43) that tensile force promotes FA assembly and stabilization. Following the classical theory of linear kinetic relation, the plaque recruitment flux J (i.e., the FA growth rate) can be related to $\Delta\mu$ as

$$J = -D\Delta\mu, \tag{14}$$

where D is a constant describing the kinetics of protein assembly. In steady state, the plaque will possess a constant size and hence $J = 0$.

The values of parameters adopted in this study along with their sources are listed in Table 1 (44–50). In addition, the physical meanings of all of the other variables in our model are also gathered in Table 2.

RESULTS AND DISCUSSION

The stiffness a cell senses increases first and then decreases as the FA grows in size

A quantity of key interest is the effective stiffness (k_{eff}) of FA-ECM complex, which physically represents the apparent mechanical stiffness of the extracellular environment that a cell senses. This parameter is plotted in Figs. 2 *A* and 3 both as a function of FA size and ECM rigidity, with the extracellular portion of the adhesion treated as either an elastic fiber or a continuous half-space. Interestingly, in both cases, k_{eff} reaches a maximum at a certain intermediate FA size. The major difference between the two descriptions is that this quantity will undergo monotonic decrease as the size of the FA further increases if ECM is modeled as a one-dimensional fiber. Conversely, when the ECM is treated as a continuous medium, k_{eff} will eventually reach a saturation value as the FA becomes very large (Fig. 2 *B*). We must point out that the overall trends of our predictions will not change if contractile force is taken to be distributed uniformly over the adhesion, instead of only acting at the right edge (refer to the Supporting Material).

To better understand this key observation, the force distribution among integrin bonds with ECM treated as an elastic fiber was examined. As shown in Fig. 2 *C*, integrins carry the load uniformly for small FAs ($L = 4L_c$), while a

TABLE 1 List of parameters used in the model

Model Parameter	Description	Typical Value	Source
E_s	substrate modulus	~1~50 kPa	typical modulus of hydrogels used as ECM (34,39)
k_s	substrate stiffness	~1–100 pN/nm	estimated collagen fiber stiffness from experiment (36,37,44)
k_c	integrin stiffness	5 pN/nm	estimated from Fisher et al. (45), of the order of pN/nm
k_p	plaque stiffness	1 pN/nm	estimated from Fisher et al. (45), of the order of pN/nm
d_c	integrin spacing	~100 nm	Cavalcanti-Adam et al. (46), 108 nm
f_0	actin pulling force without feedback	~100 pN	Mogilner and Oster (47), 0–200 pN
k_a	actin stiffness	~50 pN/nm	Kojima et al. (48), 43.7–65.3 pN/nm
β	feedback coefficient	0–1	free parameter
k_N	nuclear stiffness	10–50 pN/nm	estimated from experiment, of the order of pN/nm (49,50)
$\Delta\mu_0$	energy barrier for protein recruitment without mechanical load	10–250 k_BT	Nicolas et al. (18)

force-free region emerges at the center when the FA size reaches ~$4L_c$. For very large FAs ($L >> 4L_c$), only a region at the leading edge carries the majority of the applied force and the size of this region remains the same regardless of actual FA length. This is an inherent aspect of a shear lag loading scenario, where load penetration into an object is limited by the critical shear lag length. As such, for a given force acting on a small FA ($L = 4L_c$), larger FAs result in more integrins to evenly share the load and thus a smaller overall displacement, leading to the monotonic increase of k_{eff} with regard to the FA size. In contrast, a larger FA ($L >> 4L_c$) can be divided into an inactive and an active part, based on the integrin loading pattern, which is equivalent to two springs in series. The active part refers to the region that carries the majority of the load at the leading edge and the inactive part is the rest of the FA. Because the size of the active part is insensitive to FA length, the effective stiffness k^A of this portion is therefore a constant, as shown by the red line in Fig. 2 *D*. For the inactive part, only the ECM fiber (connecting the active part with the boundary) is under loading and thus for this region $k^I \sim EA/L^I$, where E is the fiber modulus, A is the cross-section area, and L^I is the length of the inactive portion. Because L^I increases as FAs becomes larger, the effective stiffness k^I is a monotonic decreasing function of FA size as shown by the blue line in Fig. 2 *D*. The effective stiffness of the whole FA for a large FA ($L >> 4L_c$) thus scales with $k_{\text{eff}} \sim k^I k^A/(k^I + k^A) = k^A - (k^A)^2/(k^I + k^A)$. Consider the fact that k^A is a constant and k^I decreases as FAs become larger for large FAs ($L >> 4L_c$); the overall effective stiffness will therefore decrease with increasing FA size under this limit. As such, d_c is an increasing function of FA size for small adhesion ($L = 4L_c$) but a decreasing function of FA size for large adhesion ($L >> 4L_c$), and thus reaches its maximum when FAs reach an intermediate size ($L \sim 4L_c$). When treating the ECM as a continuum elastic medium the findings are similar, except that a saturation value for d_c will be reached when the FA becomes very large (refer to the Supporting Material for details).

For large FAs, k_{eff} scales with $1/L$ (from Eqs. 6 and 7). Therefore, k_{eff} can only reach zero when the FA is infinitely large, which clearly is physiologically impossible. Furthermore, for FAs with a length of ~10 μm, approximately twofold larger than that measured in our experiments, k_{eff} remains nonvanishing. To summarize, k_{eff} defined here will assume reasonable values when the FA size is within the physiologically relevant range.

TABLE 2 Variables and their physical meaning

Model Variables	Physical Meaning
γ_s	force in the substrate (ECM)
γ_p	force in the FA plaque
L_c	characteristic length for force transmission
k_{eff}	effective stiffness of the FA-ECM complex
u_p	FA plaque displacement
u_s	substrate (ECM) displacement
u_{FA}	FA displacement at the proximal end
u_N	nuclear displacement
f_a	contractile force generated by actin
$\Delta\mu$	chemical potential difference of adding one protein complex segment to the FA plaque
J	FA plaque recruitment flux

FA plaque recruitment is divided into three regimes by two important sizes: nucleation size and stable size

The generic shape of the plaque recruitment flux J, as a function of FA size, is given in Fig. 3 *A*. An immediate observation from this prediction is that the value of J is positive only when $L_{nu} < L < L_{st}$, where L_{st} stands for the stable size of the plaque while L_{nu} can be understood as the critical size a nascent plaque must overcome to initiate elongation (i.e., minimum nucleation size). The plaque dynamics can be divided into three regimes as depicted in Fig. 3 *A*. Newly nucleated FAs with sizes smaller than L_{nu} will dissemble and eventually disappear (i.e., as described for unstable nascent focal complexes (51)). In comparison, a small FA will increase in size toward a stable length once it passes this critical value. Larger FAs ($L > L_{st}$), on the other hand, are predicted to shrink until they reach the stable size. Fig. 3 *C* shows how the rigidity of the ECM (a one-dimensional fiber) influences the growth rate of FAs. Our model suggests that the stable structure/plaque size increases monotonically as the external environment becomes

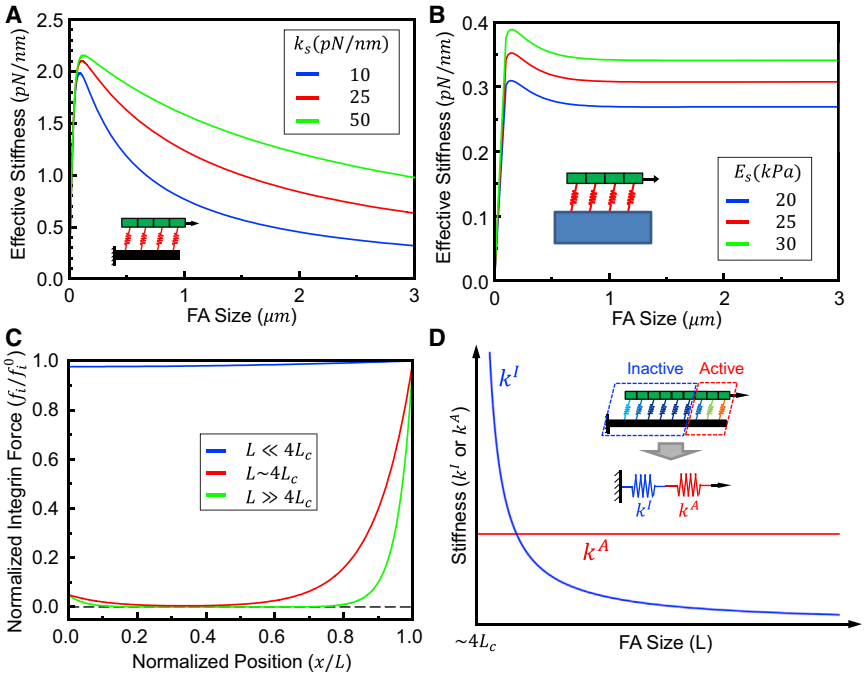

FIGURE 2 The effective stiffness of a focal adhesion as a function of its size and ECM stiffness, which in (*A*) is treated as an elastic fiber and in (*B*) is modeled as an elastic medium. (*C*) Normalized integrin force distribution ($f_i^0 = f_i(x = L)$) for FAs of different sizes. For small FAs, integrin force distributes almost uniformly. The force-free region begins to show up when FA size is comparable to $4L_c$; the leading edge carries the majority of integrin force and the size of this highly loaded region is a constant if FA size is much larger than $4L_c$. A large FA ($>>4L_c$) can be divided into two parts based on the integrin force; the effective stiffnesses of the two parts are shown, respectively, in (*D*). Note that the horizontal axis in (*D*) is starting from $L \sim 4L_c$. To see this figure in color, go online.

stiffer, in agreement with recent experimental observations (13), while the critical size decreases, indicating more adhesions would form on a stiffer environment. In addition, Fig. 3 *C* also shows that the adhesion plaque can grow faster (i.e., has a larger *J*) on a stiffer ECM for large FAs, in agreement with recent experimental findings (13). Note that, due to random factors like variations in the surface topology and chemistry of the ECM, the sizes of FAs in reality will not be uniform but are expected to be distributed around the stable value predicted here.

This nonmonotonic growth rate and FA size relation can be understood by examining the intracellular tension levels predicted by the model under each configuration. As illustrated in Eq. 11, larger contractile forces will develop when cells sense a stiffer environment, with this stiffness input originating from either a more rigid nucleus or a stiffer FA/ECM complex (Fig. 3 *B*, *top*). Consequently, our model predicts that there exists an optimum size for FA to induce maximum intracellular traction force (Fig. 3 *B*, *bottom*), corresponding to the peak value of k_{eff} shown in Fig. 2, *A* and *B*. Given that f_a is the driving force for plaque growth (refer to Eqs. 12–14), this explains why the recruitment flux *J* will be large for FAs with intermediate sizes as well as why this quantity increases with higher ECM or nuclear rigidity (Fig. 3, *A*, *C*, and *D*).

It is worth pointing out that a similar growth rate and size relationship for FAs (as illustrated in Fig. 3 *A*), as well as the conclusion that more and larger adhesions will be induced by stiffer substrates, has also been predicted by a model from Walcott et al. (30). However, unlike this study, that model treated the ECM as an array of uncoupled springs, capable of binding to integrins, and actin force was applied in the vertical direction and uniformly distributed throughout the FAs. In light of recent evidence showing that forces on FAs are almost purely tangential (31) and nonuniformly distributed (12), it appears that these assumptions are reasonable for small FAs where each integrin carries more or less the same load. As such, both this model and that of Walcott et al. (30) predict similar ECM stiffness-independent FA growth for small adhesions. However, as FAs become larger, our model shows that the tangentially applied actin force, together with a realistic treatment of the ECM (one-dimensional fiber or continuous elastic medium), will lead to load distribution in the adhesion plaque that is highly nonuniform. The size of the region for force concentration at the proximal tip of FAs depends on ECM stiffness (refer to Eq. 5), which ultimately influences the FA effective stiffness for large FAs, a feature that is not captured by the model proposed by Walcott et al. (30). From this perspective, our model may serve as a more refined and comprehensive alternative for evaluating FA growth dynamics across a range of length scales.

Cells attached to stiffer cell-derived fibrous ECM substrates build elongated adhesion structures

To validate the predicted increase in adhesion structure size, we utilized well-characterized, in vivo, mimetic-cell-derived fibrous ECMs (38,52). In this system, the physiologic difference between the cells producing the ECM results in a fibrous ECM of different stiffness (53). Isogenic human fibroblasts were used to produce the relatively soft and stiff ECMs and cells that had produced the soft ECMs were cultured overnight on both fibrous substrates. As

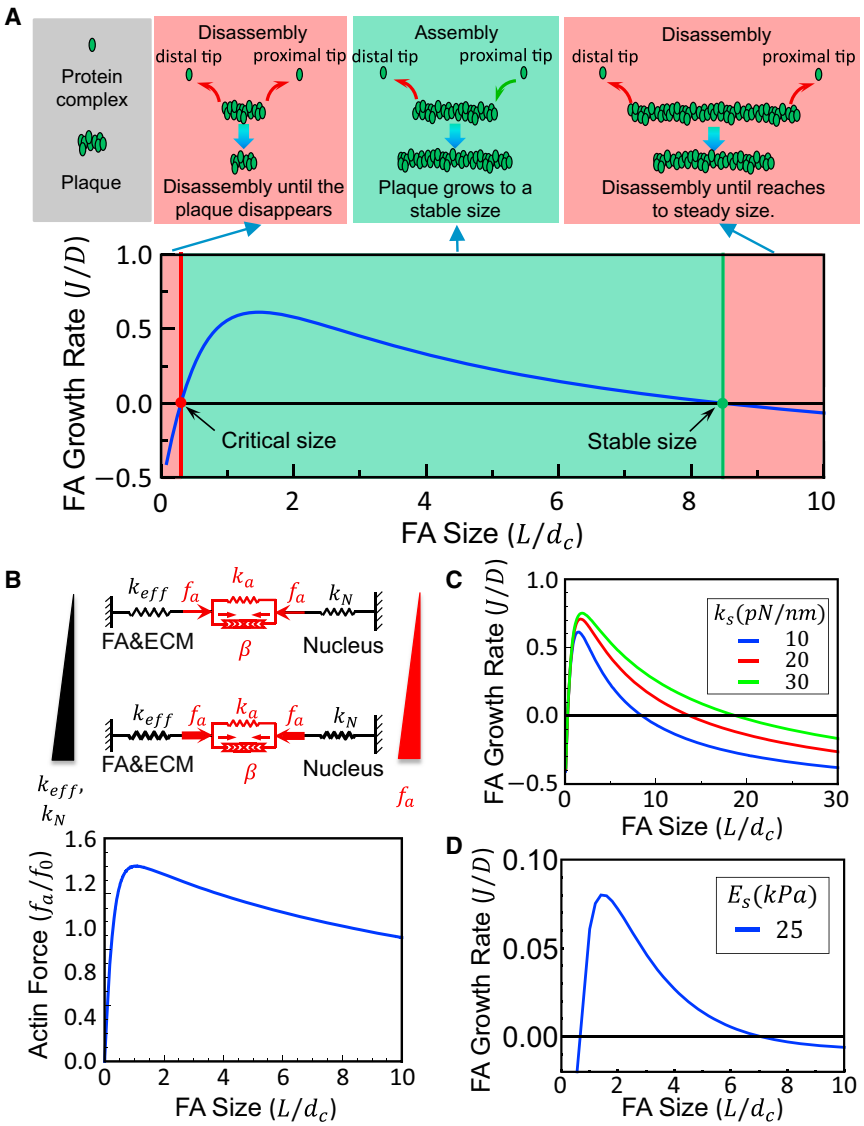

FIGURE 3 (*A*) Generic shape of the plaque recruitment flux (J) as a function of FA size, from which two quantities of central interest, i.e., the critical size for nascent adhesions develop into mature ones, and the stable size for a fully developed FA, can be identified. The value J is positive only when the plaque size is between these two values. (*B*) Higher actomyosin pulling force is induced by a stiffer ECM/FA complex and/or a more rigid nucleus (*top*); for a given surrounding environment and nuclear property, the actin force will always reach its maximum at an intermediate FA size (*bottom*). Influence of the size of FA on its growth rate on fibrous (*C*) and continuous ECM (*D*) show that larger FAs will be formed on stiffer substrates. To see this figure in color, go online.

predicted, results revealed formation of larger (45.87%, $P < 0.0001$) adhesion structures formed by cells cultured in to the relatively stiffer ECMs compared to the length of the structures formed by the same cells cultured within the softer ECM (Fig. 4, *A* and *B*). Specifically, the stable FA size predicted by our model will decrease from 5.25 to 3.5 μm when the ECM rigidities changes from 7.5 to 5 kPa (see the Supporting Material for details), which is in good agreement with our observations here (i.e., these two values were measured to be ~5.1 and 3.5 μm, respectively). Moreover, nuclei shape/deformability was observed in response to stiffening of the ECM (2–5 kPa in soft versus 5–15 kPa in stiff ECM, which simulate many normal versus tumoral microenvironments in vivo (53). Cells showed increased elliptical (18.82%, $P = 0.0005$) nuclear shape within a stiffer ECM (Fig. 4, *A* and *C*). As the model suggests that more adhesions will form on stiffer ECMs (as verified by data shown in Fig. 4 *B*), we expect that the force exerted on the nuclei will be larger on stiffer ECMs, leading to a more pronounced shape change of the nuclei; this is consistent with the experiment findings and shown in Fig. 4 *C*.

Cells with stiffer nuclei have a lower barrier for FA formation and assemble larger FAs

Our model also predicts a dependence of FA size on nuclear stiffness. As has been illustrated by several publications, some FAs are linked to basilar stress fibers, while others connect with the nucleus (54). Those that interact with the nucleus (a stiff but deformable object in the cell) are likely influenced by the structural and mechanical properties of this organelle. As shown in Fig. 5 *A*, cells that have a stiffer nucleus would be predicted to have a smaller critical FA recruitment size, meaning that the energetic barrier to FA

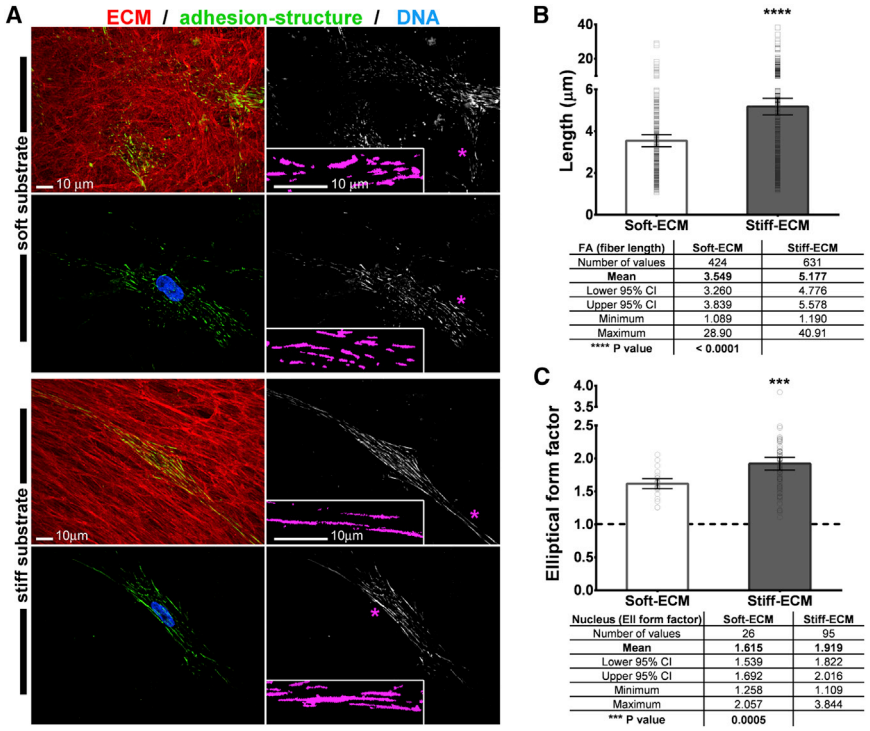

FIGURE 4 Cells form larger adhesion structures on stiffer fibrous ECM matrices. Primary human fibroblasts cultured within soft (*A*, *top two panels*), or stiff (*A*, *bottom two panels*) fibrous ECMs (*red*) display increased length of integrin-labeled adhesion structures (*green* on *left* and corresponding monochromatic on *right panels*). (*Blue*) Elongated nucleus. (*Insets*) Magnifications of digitally recognized adhesion structures (*purple*) corresponding to the areas marked (*asterisks*). Fiber length measurements of adhesion structures (i.e., FAs) revealed a larger mean for cells cultured on stiff ECM (*B*). Analysis of the elliptical (*Ell*) form factor is shown in (*C*). To see this figure in color, go online.

formation would be lower. Similarly, the model predicts that a stiffer nucleus would also lead to a larger stable FA size. It is known that the nucleus is physically connected to stress fibers via the linker-of-nucleoskeleton-and-cytoskeleton complex. One specific linker-of-nucleoskeleton-and-cytoskeleton complex component that is known to regulate force transfer to the nucleus is nesprin 1 giant (N1G) (55). To simulate the effect of decreased nuclear connectivity to the cytoskeleton (as would occur with N1G knockdown), the nucleus was removed from the model altogether (Fig. 5 *A*, N1G). Under these circumstances, the model predicts an increase in stable FA size and decrease in nucleation size.

To confirm these model-predicted results experimentally, and to determine the influence of the nucleus on FA size, nuclear connectivity to the cytoskeleton was eliminated via knockdown of N1G. Consistent with the model prediction, knockdown of N1G resulted in a significant increase in both the average size (Fig. 5 *B*) and average number (Fig. 5 *C*) of FAs in each cell. Essentially, knockdown of N1G in this context is comparable to replacing the deformable nucleus in our model with a rigid body.

Increased contractility leads to a small drop in the FA nucleation barrier and a significant increase in stable FA size

It is well documented that cell contractility is essential for the formation of FAs, independent of ECM stiffness. Our model predicts that for cells with a lower actin pulling force (i.e., weaker contractility), the nucleation barrier for FAs will be larger while their steady-state size will become smaller (Fig. 6). Our previous experimental observations (53) show that FA sizes for Cav1 knockout mouse embryonic fibroblasts (contractility-reduced cells) are significantly smaller than wild-type fibroblasts, which is consistent with our model predictions.

CONCLUSIONS

In this study, we developed a chemomechanical model to predict the growth of adhesion plaques, a process strongly influenced by the assembly of adhesion proteins as well as the stress buildup in the plaque itself (induced by actomyosin contractions). Main findings obtained here are summarized as follows:

1) FA recruitment is divided to three regimes by two quantities of key interest, i.e., the stable size and the critical size. Nascent FAs smaller than a critical size dissolve, while bigger ones grow to a mature state whose size is limited by the stable size. Meanwhile, FAs that are too large disassemble until their sizes reduce to the stable size. Using realistic parameter values, these two sizes (length along FA long axis) were predicted to be ~0.02 and ~2 μm, respectively, for NIH 3T3 fibroblasts cultured on a PAA gel substrate with shear modulus of 16 kPa, in agreement with experiments (39).
2) We quantitatively demonstrated how the aforementioned stable and nucleation sizes are influenced by the

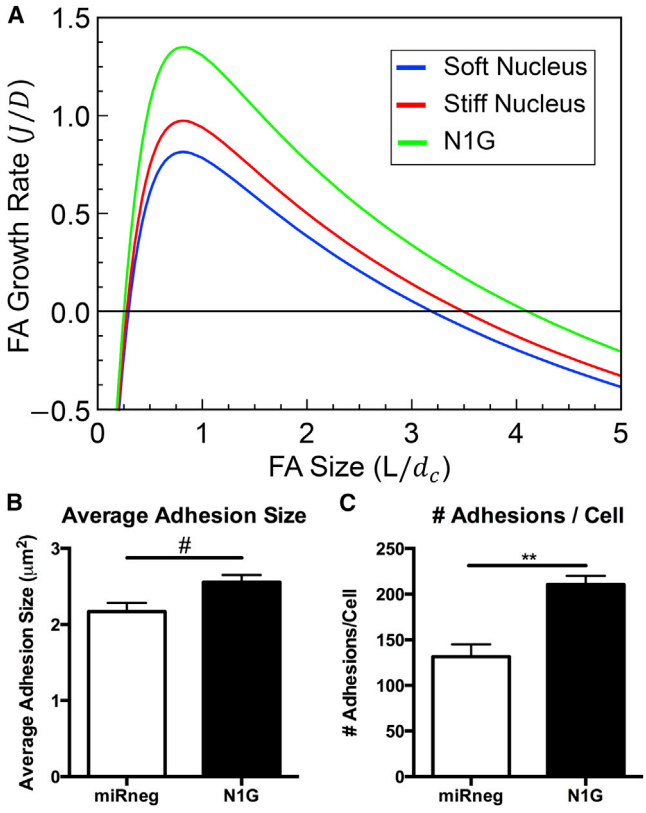

FIGURE 5 Nuclear stiffness influences maximum FA growth rate and stable size (*A*). Adhesion average size (*B*) and adhesions per cell (*C*) both increase for N1G knockdown cells. Decoupling the actin pulling force and the deformable nucleus results in an increase in both average adhesion size and number of FAs per cell. Mean ± SE, # $p < 0.05$, ** $p < 0.01$, $n = 7$–10 cells/group. To see this figure in color, go online.

incorporation dynamics of adhesion proteins as well as the deformability of the substrate, the nucleus, and the plaque itself. In particular, we found that a stiffer substrate will lead to bigger plaques. In addition, with increasing substrate rigidity, more adhesions are predicted to form as a result of the diminishing nucleation size. These predictions are consistent with our experimental results (as shown in Fig. 4, *A*–*C*) and other existing results in literature (12,14). As for nucleus stiffness, similar effects were found, where a stiffer nucleus led to a larger FA stable size and a smaller critical size. Again, this conclusion is verified by our experiments as shown in Fig. 5.

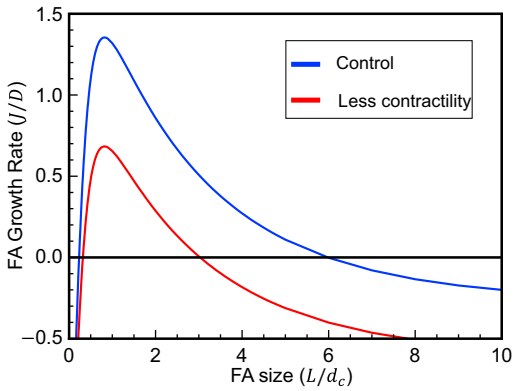

FIGURE 6 Increased contractility results in larger stable FAs and a smaller FA nucleation barrier. To see this figure in color, go online.

TABLE 3 Influence of key parameters on the characteristics of FAs

FA Characteristics	Key Parameters
L_{nu}, FA critical size	k_s, ECM stiffness (−); k_N, nucleus stiffness (−); f_0, contractility (−)
L_{st}, FA stable size	k_s, ECM stiffness (+); k_N, nucleus stiffness (+); f_0, contractility (+)
Number of FAs	k_s, ECM stiffness (+); k_N, nucleus stiffness (+); f_0, contractility (+)

The plus (+) sign means the corresponding characteristic is increasing with the increase of the parameter, and vice versa for the minus (−) sign.

3) Interestingly, the model also predicts that the growth of the plaque is significantly influenced by contractility (see the Supporting Material). Specifically, high levels of contractility will lead to bigger plaques, which is in agreement with previous observations (53). Additionally, more adhesions are expected with increasing contractility, due to the decreasing nucleation size. These predictions compare favorably with the findings that low contractility leads to decreased vinculin recruitment (56).

To make these predictions/findings transparent, the influence of key parameters on the formation of FAs is gathered in Table 3.

We believe that this model can also be used to study phenomena such as cell locomotion (57) and stretch-induced cell reorientation (58,59), where forces generated inside the cell and the turnover of FAs are known to play pivotal roles; indeed efforts along these lines, as of this writing, are underway.

SUPPORTING MATERIAL

Supporting Materials and Methods and seven figures are available at http://www.biophysj.org/biophysj/supplemental/S0006-3495(15)00936-4.

AUTHOR CONTRIBUTIONS

V.B.S. conceived the model; X.C., Y.L. and V.B.S. formulated the mathematical framework; X.C. carried out the computations; T.P.D., J.F.-B., E.C., and R.L.M. designed the experiments; T.P.D. and J.F.-B. conducted the experiments; and X.C., Y.L., T.P.D., J.F.-B., E.C., R.L.M., and V.B.S. wrote the article.

ACKNOWLEDGMENTS

Research reported in this publication was supported by the National Institutes of Health with funds from the National Institute of Biomedical

Imaging and Bioengineering under award Nos. R01EB017753 (to V.B.S.) and R01EB002425 (to R.L.M.); the National Cancer Institute under award Nos. U01CA202177, U54CA193417 (to V.B.S.), and R01CA113451 (to E.C.); and the U.S. National Science Foundation under grant No. CMMI-1312392 (to V.B.S.). Additional support was provided by a University Research Foundation Award from the University of Pennsylvania (to V.B.S. and R.L.M.) and an appropriation from the state of Pennsylvania to the Fox Chase Cancer Center (P30-CA006927).

SUPPORTING CITATIONS

Refs. (60,61) appear in the Supporting Material.

REFERENCES

1. Nelson, C. M., R. P. Jean, …, C. S. Chen. 2005. Emergent patterns of growth controlled by multicellular form and mechanics. *Proc. Natl. Acad. Sci. USA.* 102:11594–11599.
2. Engler, A. J., S. Sen, …, D. E. Discher. 2006. Matrix elasticity directs stem cell lineage specification. *Cell.* 126:677–689.
3. Janmey, P. A., J. P. Winer, …, Q. Wen. 2009. The hard life of soft cells. *Cell Motil. Cytoskeleton.* 66:597–605.
4. Kanchanawong, P., G. Shtengel, …, C. M. Waterman. 2010. Nanoscale architecture of integrin-based cell adhesions. *Nature.* 468:580–584.
5. Gorfinkiel, N., G. B. Blanchard, …, A. Martinez Arias. 2009. Mechanical control of global cell behaviour during dorsal closure in *Drosophila*. *Development.* 136:1889–1898.
6. Mammoto, T., and D. E. Ingber. 2010. Mechanical control of tissue and organ development. *Development.* 137:1407–1420.
7. Kumar, S., and V. M. Weaver. 2009. Mechanics, malignancy, and metastasis: the force journey of a tumor cell. *Cancer Metastasis Rev.* 28:113–127.
8. Paszek, M. J., N. Zahir, …, V. M. Weaver. 2005. Tensional homeostasis and the malignant phenotype. *Cancer Cell.* 8:241–254.
9. Fenteany, G., P. A. Janmey, and T. P. Stossel. 2000. Signaling pathways and cell mechanics involved in wound closure by epithelial cell sheets. *Curr. Biol.* 10:831–838.
10. Oakes, P. W., Y. Beckham, …, M. L. Gardel. 2012. Tension is required but not sufficient for focal adhesion maturation without a stress fiber template. *J. Cell Biol.* 196:363–374.
11. Riveline, D., E. Zamir, …, A. D. Bershadsky. 2001. Focal contacts as mechanosensors: externally applied local mechanical force induces growth of focal contacts by an mDia1-dependent and ROCK-independent mechanism. *J. Cell Biol.* 153:1175–1186.
12. Plotnikov, S. V., A. M. Pasapera, …, C. M. Waterman. 2012. Force fluctuations within focal adhesions mediate ECM-rigidity sensing to guide directed cell migration. *Cell.* 151:1513–1527.
13. Trichet, L., J. Le Digabel, …, B. Ladoux. 2012. Evidence of a large-scale mechanosensing mechanism for cellular adaptation to substrate stiffness. *Proc. Natl. Acad. Sci. USA.* 109:6933–6938.
14. Peyton, S. R., and A. J. Putnam. 2005. Extracellular matrix rigidity governs smooth muscle cell motility in a biphasic fashion. *J. Cell. Physiol.* 204:198–209.
15. Guo, W. H., M. T. Frey, …, Y. L. Wang. 2006. Substrate rigidity regulates the formation and maintenance of tissues. *Biophys. J.* 90:2213–2220.
16. Lele, T. P., J. Pendse, …, D. E. Ingber. 2006. Mechanical forces alter zyxin unbinding kinetics within focal adhesions of living cells. *J. Cell. Physiol.* 207:187–194.
17. Shemesh, T., B. Geiger, …, M. M. Kozlov. 2005. Focal adhesions as mechanosensors: a physical mechanism. *Proc. Natl. Acad. Sci. USA.* 102:12383–12388.
18. Nicolas, A., B. Geiger, and S. A. Safran. 2004. Cell mechanosensitivity controls the anisotropy of focal adhesions. *Proc. Natl. Acad. Sci. USA.* 101:12520–12525.
19. Nicolas, A., and S. A. Safran. 2006. Limitation of cell adhesion by the elasticity of the extracellular matrix. *Biophys. J.* 91:61–73.
20. Lin, Y., and L. B. Freund. 2008. Optimum size of a molecular bond cluster in adhesion. *Phys. Rev. E Stat. Nonlin. Soft Matter Phys.* 78:021909.
21. Qian, J., J. Wang, …, H. Gao. 2009. Lifetime and strength of periodic bond clusters between elastic media under inclined loading. *Biophys. J.* 97:2438–2445.
22. Zhang, W., Y. Lin, …, H. Gao. 2013. Tuning molecular adhesion via material anisotropy. *Adv. Funct. Mater.* 23:4729–4738.
23. Nicolas, A., A. Besser, and S. A. Safran. 2008. Dynamics of cellular focal adhesions on deformable substrates: consequences for cell force microscopy. *Biophys. J.* 95:527–539.
24. Paszek, M. J., D. Boettiger, …, D. A. Hammer. 2009. Integrin clustering is driven by mechanical resistance from the glycocalyx and the substrate. *PLOS Comput. Biol.* 5:e1000604.
25. Chan, C. E., and D. J. Odde. 2008. Traction dynamics of filopodia on compliant substrates. *Science.* 322:1687–1691.
26. Bangasser, B. L., S. S. Rosenfeld, and D. J. Odde. 2013. Determinants of maximal force transmission in a motor-clutch model of cell traction in a compliant microenvironment. *Biophys. J.* 105:581–592.
27. Zamir, E., B. Z. Katz, …, Z. Kam. 1999. Molecular diversity of cell-matrix adhesions. *J. Cell Sci.* 112:1655–1669.
28. Dugina, V., L. Fontao, …, G. Gabbiani. 2001. Focal adhesion features during myofibroblastic differentiation are controlled by intracellular and extracellular factors. *J. Cell Sci.* 114:3285–3296.
29. Choi, C. K., M. Vicente-Manzanares, …, A. R. Horwitz. 2008. Actin and α-actinin orchestrate the assembly and maturation of nascent adhesions in a myosin II motor-independent manner. *Nat. Cell Biol.* 10:1039–1050.
30. Walcott, S., D.-H. Kim, …, S. X. Sun. 2011. Nucleation and decay initiation are the stiffness-sensitive phases of focal adhesion maturation. *Biophys. J.* 101:2919–2928.
31. Legant, W. R., C. K. Choi, …, C. S. Chen. 2013. Multidimensional traction force microscopy reveals out-of-plane rotational moments about focal adhesions. *Proc. Natl. Acad. Sci. USA.* 110:881–886.
32. Kim, D.-H., and D. Wirtz. 2013. Focal adhesion size uniquely predicts cell migration. *FASEB J.* 27:1351–1361.
33. Goffin, J. M., P. Pittet, …, B. Hinz. 2006. Focal adhesion size controls tension-dependent recruitment of α-smooth muscle actin to stress fibers. *J. Cell Biol.* 172:259–268.
34. Trappmann, B., J. E. Gautrot, …, W. T. Huck. 2012. Extracellular-matrix tethering regulates stem-cell fate. *Nat. Mater.* 11:642–649.
35. Wen, J. H., L. G. Vincent, …, A. J. Engler. 2014. Interplay of matrix stiffness and protein tethering in stem cell differentiation. *Nat. Mater.* 13:979–987.
36. Matthews, J. A., G. E. Wnek, …, G. L. Bowlin. 2002. Electrospinning of collagen nanofibers. *Biomacromolecules.* 3:232–238.
37. Keene, D. R., L. Y. Sakai, …, R. E. Burgeson. 1987. Type III collagen can be present on banded collagen fibrils regardless of fibril diameter. *J. Cell Biol.* 105:2393–2402.
38. Cukierman, E., R. Pankov, …, K. M. Yamada. 2001. Taking cell-matrix adhesions to the third dimension. *Science.* 294:1708–1712.
39. Stricker, J., Y. Aratyn-Schaus, …, M. L. Gardel. 2011. Spatiotemporal constraints on the force-dependent growth of focal adhesions. *Biophys. J.* 100:2883–2893.
40. Johnson, K. L. 1985. Contact Mechanics. Cambridge University Press, New York.
41. Zemel, A., F. Rehfeldt, …, S. A. Safran. 2010. Optimal matrix rigidity for stress fiber polarization in stem cells. *Nat. Phys.* 6:468–473.

42. Besser, A., and U. S. Schwarz. 2007. Coupling biochemistry and mechanics in cell adhesion: a model for inhomogeneous stress fiber contraction. *New J. Phys.* 9:425.

43. Grashoff, C., B. D. Hoffman, …, M. A. Schwartz. 2010. Measuring mechanical tension across vinculin reveals regulation of focal adhesion dynamics. *Nature.* 466:263–266.

44. Gentleman, E., A. N. Lay, …, K. C. Dee. 2003. Mechanical characterization of collagen fibers and scaffolds for tissue engineering. *Biomaterials.* 24:3805–3813.

45. Fisher, T. E., A. F. Oberhauser, …, J. M. Fernandez. 1999. The study of protein mechanics with the atomic force microscope. *Trends Biochem. Sci.* 24:379–384.

46. Cavalcanti-Adam, E. A., A. Micoulet, …, J. P. Spatz. 2006. Lateral spacing of integrin ligands influences cell spreading and focal adhesion assembly. *Eur. J. Cell Biol.* 85:219–224.

47. Mogilner, A., and G. Oster. 2003. Force generation by actin polymerization II: the elastic ratchet and tethered filaments. *Biophys. J.* 84:1591–1605.

48. Kojima, H., A. Ishijima, and T. Yanagida. 1994. Direct measurement of stiffness of single actin filaments with and without tropomyosin by in vitro nanomanipulation. *Proc. Natl. Acad. Sci. USA.* 91:12962–12966.

49. Caille, N., O. Thoumine, …, J.-J. Meister. 2002. Contribution of the nucleus to the mechanical properties of endothelial cells. *J. Biomech.* 35:177–187.

50. Mathur, A. B., W. M. Reichert, and G. A. Truskey. 2007. Flow and high affinity binding affect the elastic modulus of the nucleus, cell body and the stress fibers of endothelial cells. *Ann. Biomed. Eng.* 35:1120–1130.

51. Cukierman, E., R. Pankov, and K. M. Yamada. 2002. Cell interactions with three-dimensional matrices. *Curr. Opin. Cell Biol.* 14:633–639.

52. Castelló-Cros, R., and E. Cukierman. 2009. Stromagenesis during tumorigenesis: characterization of tumor-associated fibroblasts and stroma-derived 3D matrices. *Methods Mol. Biol.* 522:275–305.

53. Goetz, J. G., S. Minguet, …, M. A. Del Pozo. 2011. Biomechanical remodeling of the microenvironment by stromal caveolin-1 favors tumor invasion and metastasis. *Cell.* 146:148–163.

54. Chancellor, T. J., J. Lee, …, T. Lele. 2010. Actomyosin tension exerted on the nucleus through nesprin-1 connections influences endothelial cell adhesion, migration, and cyclic strain-induced reorientation. *Biophys. J.* 99:115–123.

55. Lombardi, M. L., D. E. Jaalouk, …, J. Lammerding. 2011. The interaction between nesprins and sun proteins at the nuclear envelope is critical for force transmission between the nucleus and cytoskeleton. *J. Biol. Chem.* 286:26743–26753.

56. Dumbauld, D. W., H. Shin, …, A. J. García. 2010. Contractility modulates cell adhesion strengthening through focal adhesion kinase and assembly of vinculin-containing focal adhesions. *J. Cell. Physiol.* 223:746–756.

57. Pelham, R. J., Jr., and Yl. Wang. 1997. Cell locomotion and focal adhesions are regulated by substrate flexibility. *Proc. Natl. Acad. Sci. USA.* 94:13661–13665.

58. Qian, J., H. Liu, …, H. Gao. 2013. A mechanochemical model of cell reorientation on substrates under cyclic stretch. *PLoS One.* 8:e65864.

59. Ao, M., B. M. Brewer, …, D. Li. 2015. Stretching fibroblasts remodels fibronectin and alters cancer cell migration. *Sci. Rep.* 5:8334.

60. Doyle, A. D., M. L. Kutys, …, K. M. Yamada. 2012. Micro-environmental control of cell migration—myosin IIA is required for efficient migration in fibrillar environments through control of cell adhesion dynamics. *J. Cell Sci.* 125:2244–2256.

61. Beacham, D. A., M. D. Amatangelo, and E. Cukierman. 2007. Preparation of extracellular matrices produced by cultured and primary fibroblasts. *Curr. Protoc. Cell Biol.* Chapter 10, Unit 10.9.

Supporting Material

A Chemomechanical Model of Matrix and Nuclear Rigidity Regulation of Focal Adhesion Size

Xuan Cao,[1] Yuan Lin,[2] Tristian P. Driscoll,[3] Janusz Franco-Barraza,[4] Edna Cukierman,[4] Robert L. Mauck,[3,5] and Vivek B. Shenoy[1,5,*]

[1]Department of Materials Science and Engineering, School of Engineering and Applied Science, The University of Pennsylvania, Philadelphia, Pennsylvania; [2]Department of Mechanical Engineering, The University of Hong Kong, Hong Kong SAR, China; [3]Department of Orthopaedic Surgery, Perelman School of Medicine, University of Pennsylvania, Philadelphia, Pennsylvania; [4]Cancer Biology Program, Fox Chase Cancer Center, Temple Health, Philadelphia, Pennsylvania; and [5]Department of Bioengineering, School of Engineering and Applied Science, University of Pennsylvania, Philadelphia, Pennsylvania

Experimental Methods

Cell-derived ECM based 3D cultures and indirect immunofluorescence

Cell derived ECMs were obtained as published (1, 2). Briefly, control and desmoplastic fibroblasts were seeded at a confluent cell concentration (i.e., 250,000 cells/ml) onto 0.2% gelatin pre-coated coverslips. Culture media was supplemented with 50 μg/ml ascorbic acid every 24 h during an ECM production period lasting 8 days. ECMs were denuded from cells using an alkaline detergent treatment (0.5% Triton X-100, 20 mM NH4OH in PBS) rendering the assorted ECMs. Naive (i.e., inactivated) fibroblasts were cultured overnight within the assorted ECMs. Cells were fixed/permeabilized as published (1) and indirectly labeled for fibronectin (ECM; in red) or DNA (blue) and alpha5beta1 integrin (3D adhesion structures; in green, monochromatic or digitally highlighted in purple). Images were obtained using a spinning disc confocal microscope with a CFI Apo TIRF 60X Oil objective. Images were acquired at 0.5 μm thick sequential Z planes and a maximum reconstructed projection was provided for the digital imaging analyses using the Offline complete MetaMorph V7.8 software (Molecular Devices, Downingtown, PA). Identical fluorescence intensity thresholds were set for both conditions in order to facilitate adhesion structure selections which were analyzed using the software's integrated morphometric analysis rendering adhesion structure numbers and fiber length of assorted objects (adhesion plaques), expressed in microns. The nuclear shape was determined by calculating the elliptical (Ell) form factor of selected objects (i.e., DNA stained nuclei). *Elliptical Form Factor = length/breadth;* an Ell-FF ratio value of 1 corresponds to a circular shape while numbers greater than 1 represent increasingly elongated nuclear shapes.

Adhesion size depends on nuclear stiffness

To experimentally determine the impact of the nucleus on adhesion size, nuclear connectivity to the cytoskeleton was experimentally perturbed in primary bovine mesenchymal stem cells and adhesion size and number was quantified. For this, knockdown of the LINC complex component nesprin 1 giant was performed using miRNA delivered via lentivirus (Block-it Lentiviral Pol II miR RNAi Expression System with EmGFP, Invitrogen). Three nesprin 1 giant vectors were designed and the miRNA sequence that resulted in the highest levels of knockdown (verified by dot blot for nesprin 1 following 1MDa size filtration) was used (TGCCGAGGACCTTCATCTTCT). Cells were infected with virus overnight, trypsinized 4 days post infection, and re-seeded on glass. The following day, cells seeded on glass slides were fixed and permeablized simultaneously using microtubule stabilizing buffer for 10 minutes at 37°C (0.1M PIPES pH6.75, 1mM EGTA, 1mM $MgSO_4$, 4% w/v polyethylene glycol, 1% Triton X-100, 2% paraformaldehyde), then washed with PBS and stained with anti-vinculin antibody (1:200, Sigma) in 1% w/v BSA in PBS overnight at 4°C. Cells were then washed 3 times with PBS, and then incubated for 60 min at room temperature with Alexa-fluor 546 goat anti-mouse secondary (Molecular Probes, 1:200). Stained cells were washed 3 times and mounted with DAPI containing mounting medium (ProLong Gold Antifade Reagent, Molecular Probes). Images were acquired using a Nikon A1 laser scanning confocal microscope with 20X objective. Z-stacks were acquired at 0.75μm slice thickness over the entire cell with the slice at the base of the cell used for quantification of adhesion size and number. Background subtracted images were converted to binary and adhesions were quantified for each cell (n=7-11 cells per group) using the analyze particles function in ImageJ.

Model descriptions

Boundary conditions for FAs on ECM fibers

As discussed in literature (3, 4), cells are likely to form entire FA on one single fiber *in vivo* as shown in Fig. A1. As actomyosin is pulling the FA to the right, the left side of the ECM fiber is under tension while the right side is under compression. As we know that a fiber of length l under compression would buckle above a critical force (F_{cr}), given by,

$$F_{cr} = \frac{\pi^2 EI}{(Kl)^2} \tag{S1}$$

where E is Young's modulus of the fiber, I is area moment of inertia and K is the column effective length factor. For a typical Collagen-I fibers ($r{\sim}50\ nm$, $l{\sim}30\ \mu m$, $E{\sim}300\ MPa$) (5, 6), from Eq. (S1), the critical buckling force is around 16 pN, which is far smaller than the actomyosin pulling force (around 100 pN) (7). Thus, when a FA forms on the ECM fiber, the right part will buckle, and the fiber provides very small resistance. So for the right boundary is treated as a traction-free edge, or, $du_s/dx|_{x=L} = 0$.

If FA does not start forming at the left edge of the ECM fiber, but from a position at $x = L_l$ (as shown in Fig. A1), this is equivalent to adding a new spring (the stiffness is related to L_l) to the left end of ECM fibers in our existing model. This change would make the effective stiffness (k_{eff}) smaller than the case when FA starts forming at the left end of ECM fiber at a given FA size, but will still show the non-monotonic relation (increasing first then decreasing) with respect to the FA size (L). As a result, our main conclusions will still hold. To better understand the physics and make predictions, we assume that the FA starts forming at the left end of ECM fiber ($L_l = 0$), which allows us to obtain analytical results. Meanwhile, we need to point out that L_l can range from zero to the total length of the fiber. As discussed above, the randomness of this length will result in change in k_{eff} and thus lead to different stable FA sizes. If $L_l = 0$, the stable

size will be the value predicted by our model; if L_l is too large, the stable size will be zero because the local ECM stiffness is too soft for the cell to form FAs at this position. Thus our results provide an upper bound on the FA size.

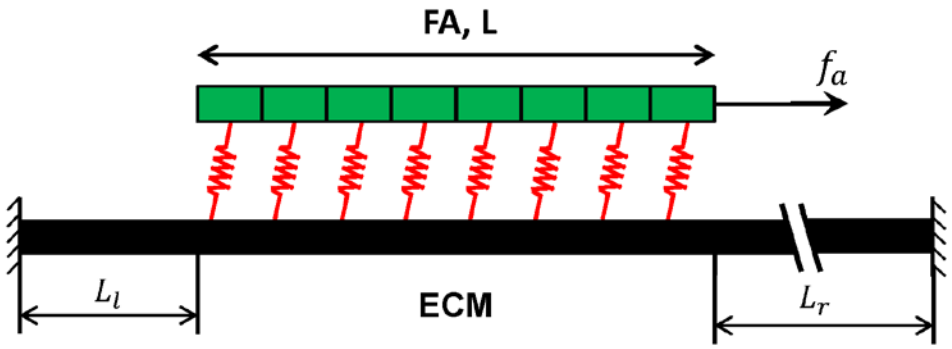

Figure S1: Schematics of FA on an ECM fiber.

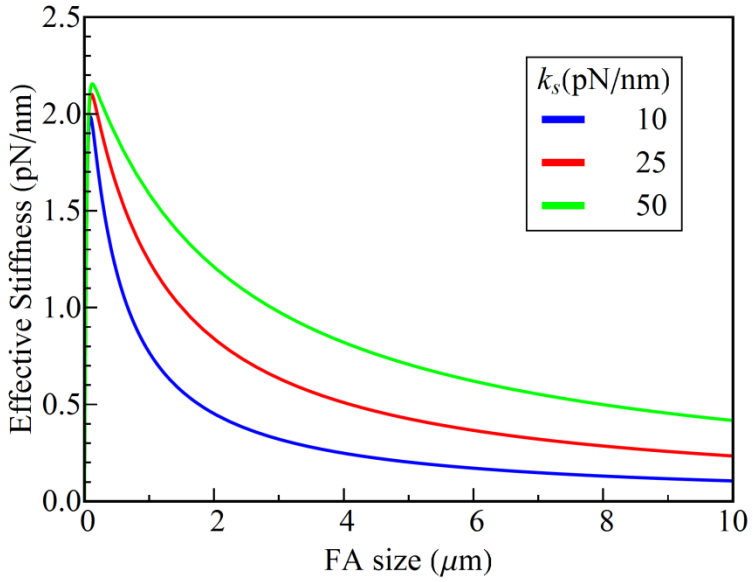

Figure S2: Effective stiffness of FA as a function of FA size and ECM stiffness, plotted in a larger scale.

Governing equations for a continuum representation of the ECM

The equation governing the deformation of the plaque remains the same even if the extracellular side changes from an elastic fiber to a continuous medium, that is

$$k_p d_c^2 \frac{d^2 u_p}{dx^2} = \gamma_c(x) \tag{S2}$$

with $\gamma_c(x)$ being the integrin force at position x which, similar to before, can be expressed as

$$\gamma_c(x) = k_c(u_p(x) - u_s(x)). \tag{S3}$$

To determine the substrate deformation u_s in this case, recall that from the Green's function for an elastic half-space, the surface deflection $u_s^t(x)$ induced by a unit point force at position t is (8)

$$u_s^t(x) = \frac{1+\nu}{\pi E_s}\frac{1}{|x-t|} \tag{S4}$$

where E_s and ν are the Young's modulus and Poisson's ratio of the substrate respectively. By using the principle of superposition, the integrin-force induced substrate displacement can be obtained as

$$u_s(x) = \int_0^L \frac{1+\nu}{\pi E_s}\frac{1}{|x-t|}\gamma_c dt. \tag{S5}$$

Numerical solution of elastic fields with COMSOL

In this study, the finite element package COSMOL was used to solve the problem shown in Fig. 1d. Specifically, a slender elastic fiber and another elastic body, with much larger dimensions, were introduced to represent the adhesion plaque and the substrate, respectively. To simplify the problem, only half of the model was built in COMSOL with symmetric boundary conditions (Fig. S3(a)). These two parts were connected to each other by a series of springs, representing the integrin bonds. During the simulation, a controlled horizontal pulling force was applied on one end of the plaque and the corresponding deformation generated (i.e. the displacement field within the plaque) was then calculated and recorded (refer to Fig. S3(b)), from which the effective stiffness of the FA (defined in Eq. (6)) can be extracted. Results for a denser mesh model are also shown in Fig. S3(b), which provide similar results and indicate that the mesh size used was sufficiently dense.

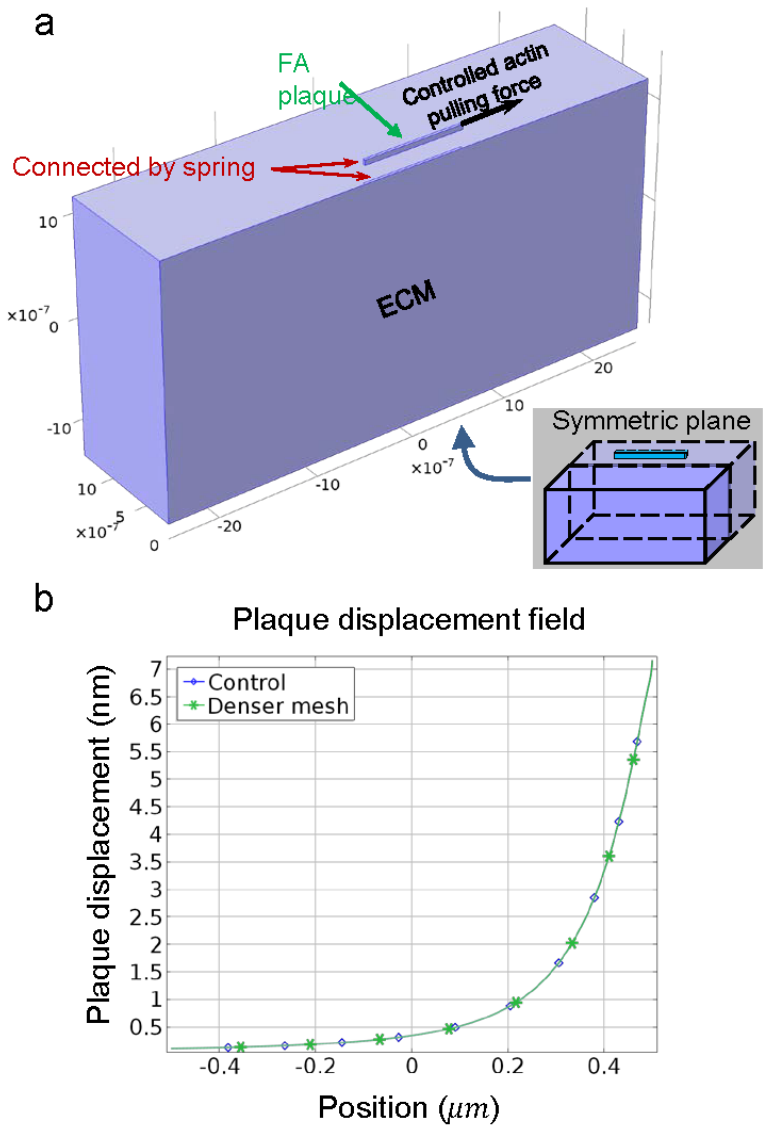

Figure S3: (a) – A computational model built in COMSOL. (b) – A representative simulation result showing the deformation of the plaque with the mesh size used (blue) and a denser mesh (green).

Model predictions

Quantitative comparison between model predictions and experimental results

Note that the rigidities of fibrous ECMs used in our experiments (as shown in Fig. 4) have been measured to be ~7.5 kPa and 5 kPa for the stiff and soft substrates (9), respectively. In addition, the mesh spacing was also observed to be in the range 5 to 15 μm. Relating the fiber stiffness to

the measured modulus and mesh size through the relation, $k_s \approx EL_{mesh}$, yields an effective fiber stiffness of the order of 25-75 pN/nm and 37.5-112.5 pN/nm for the two cases. Using these values and other parameters from Table 1, the stable FA size is predicted to be in the range of 1.8-5.2 μm (median is 3.5 μm) vs 2.7-7.8 μm (median is 5.25 μm) for the soft and the stiff ECMs respectively, which is in good agreement with experimental measurements (3.5 μm vs 5.1 μm for mean FA length as shown in Fig. 4).

Influence of the force distribution acting on the adhesion plaque

To examine whether the distribution of contractile force acting on the adhesion plaque will significantly influence the model predictions, we also considered the case where the force is assumed to be evenly distributed over the whole adhesion plaque .In this case, Eq. 3 should be modified as,

$$\begin{cases} k_p d_c^2 \dfrac{d^2 u_p}{dx^2} = k_c(u_p - u_s) - p \\ k_s d_c^2 \dfrac{d^2 u_s}{dx^2} = -k_c(u_p - u_s) \end{cases}$$

where p represents the force acting on adhesion per unit length. This equation is then solved with similar boundary conditions given in the Section 'METHODS-Model Formulation: Mechanical response of the system', from which the effective stiffness of a FA can be calculated. We find that the effective stiffness first increases and then decreases with respect to the FA size (Fig. S4). In addition, a stiffer ECM also leads to an overall increase of effective stiffness of FAs. Therefore, we do not find any qualitative changes when the nature of the way in which actin force is transmitted through the adhesion plaque is altered.

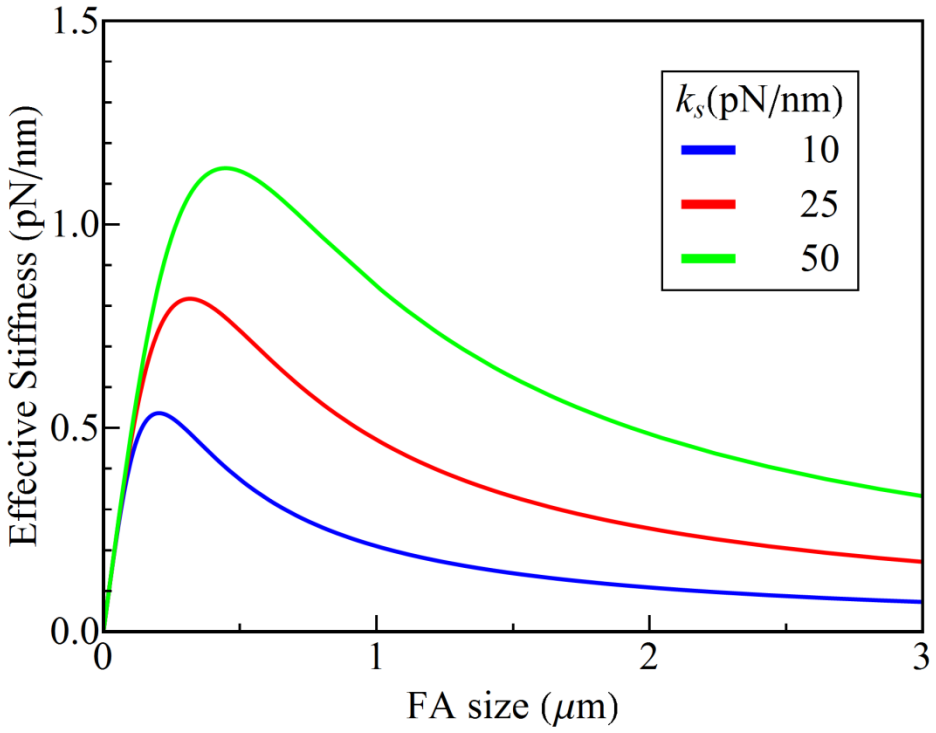

Figure S4: Effective stiffness of a FA as a function of its size and ECM stiffness under the assumption that the contraction force is distributed uniformly across the FA plaque.

Sensitivity of the predictions to model parameters

A parametric study was carried out to demonstrate how our model predictions are influenced by the plaque (Fig. S5a) and integrin stiffnesses (Fig. S5b). Clearly, variations in k_p and k_c will affect the effective stiffness of a FA and eventually change its growth rate. However, the predicted steady-state size of FAs is less sensitive to these variations (they remain with a few micrometers of each other) as shown in the figure below.

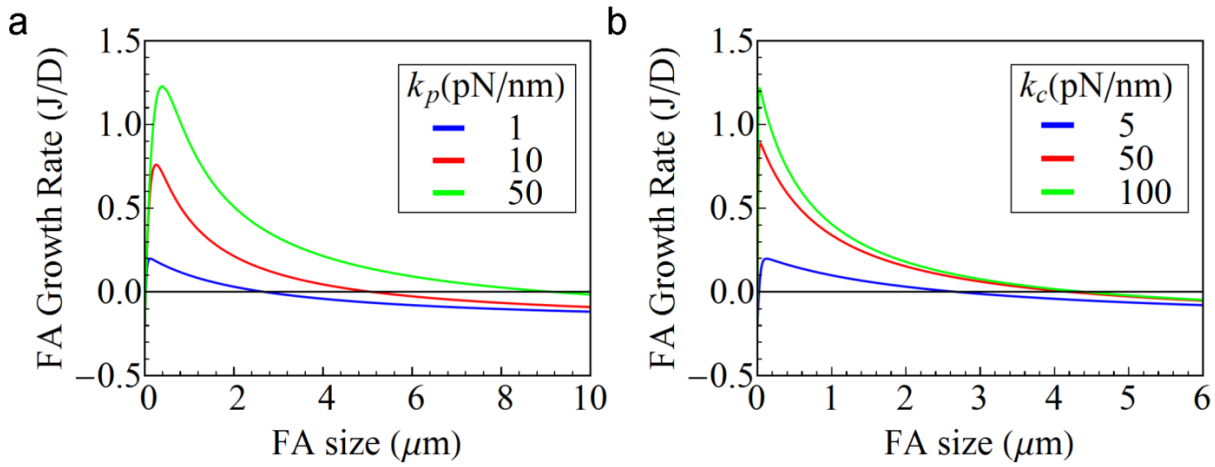

Figure S5: The growth rate of a FA as a function of its size for different plaque (a) and integrin stiffnesses (b).

We have also investigated the dependence of the growth rate – size relationship on the spacing between integrins. Interestingly, as shown in Fig. S6, a larger integrin spacing results in significantly increased critical size, stable size as well as growth rate of FAs, suggesting that it would be harder for the mature adhesions to form. This prediction are consistent with experimental findings that show fewer focal attachments with the ECM when the integrin spacing becomes larger (10).

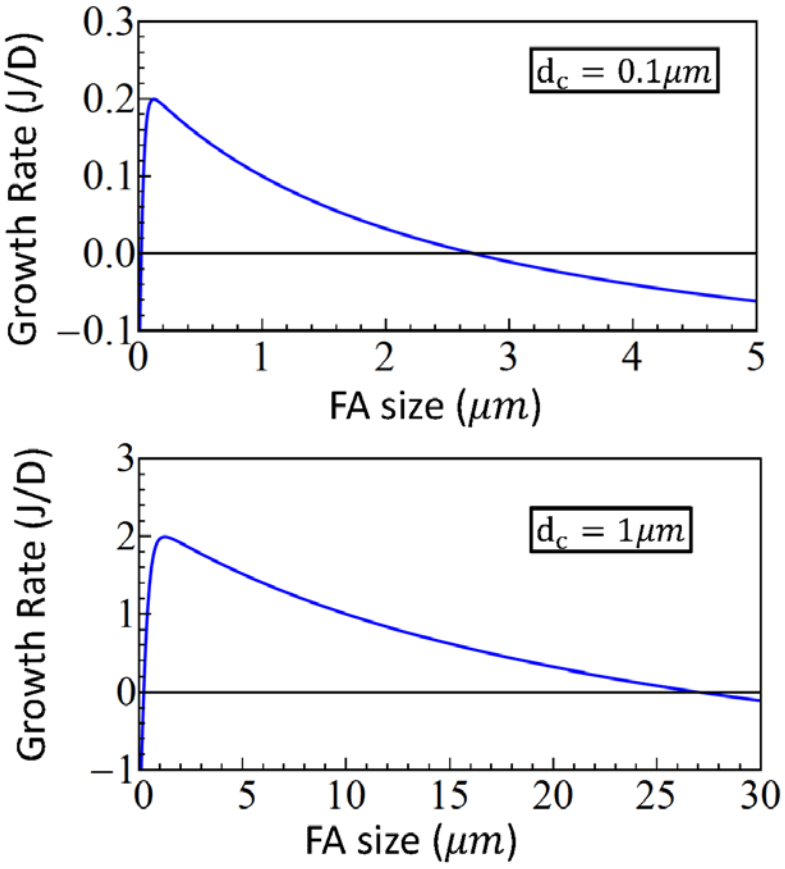

Figure S6: The growth rate – size relationship of FAs for different integrin spacings.

The way that force transmission leads to saturation of k_{eff} when treating the ECM as a continuum elastic medium.

The force distribution among integrin bonds, connecting the adhesion plaque to the elastic half-space (i.e. the ECM) was examined. As shown in Fig. S7, integrins carry the load evenly for small FAs ($L \ll 4L_c$) and hence the force shared by each integrin decreases as more integrins get engaged (i.e. as the FA becomes larger), which results in a smaller deformation of both integrins and the ECM. In this regime, the effective stiffness k_{eff} of a FA increases as it grows. Fig. S7 also demonstrates that the load distribution near the edge of a large FA ($L \gg 4L_c$) actually becomes insensitive to its size (with interior integrin clutches carrying basically zero load).

Given that in this case the actin force is transmitted through an infinite elastic medium (not a 1D fiber with length scale with the FA size), the displacement field in ECM is therefore insensitive to how big the FA is, which corresponds to the saturation value of k_{eff} observed in Fig. 2b.

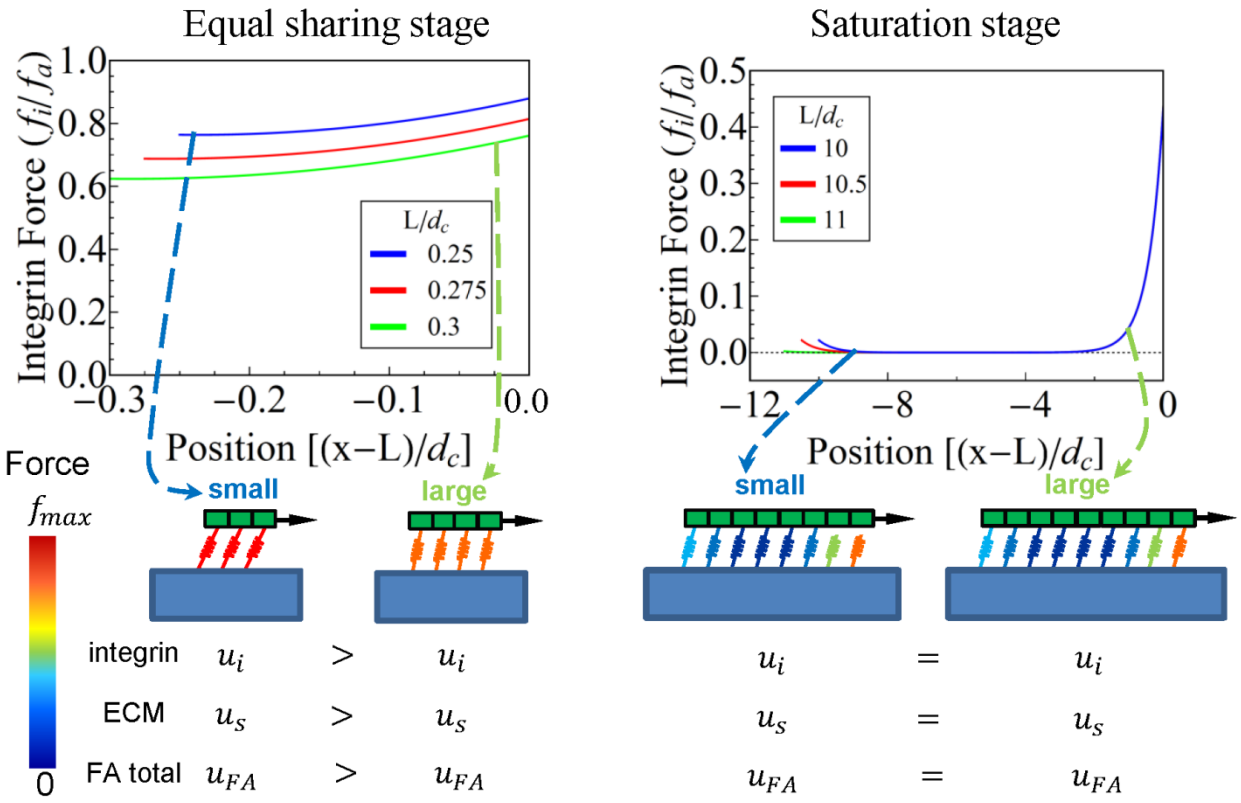

Figure S7: For small FAs ($L \ll 4L_c$), force is almost equally shared by integrins. A larger FA in this regime will lead to lower force on each integrin, resulting in a decreased integrin and ECM displacement at the edge, and hence a monotonic increase of k_{eff}. For very large FAs ($L \gg 4L_c$), integrin force is concentrated in a limited region at their leading edges while the distribution of integrin force is insensitive to FA size. The displacement field of ECM is therefore independent of how big the FA is, leading to a saturated value of k_{eff}. Notice all displacements given here are measured at the right edge (i.e. x=L).

SUPPORTING REFERENCES

1. Castelló-Cros, R., and E. Cukierman. 2009. Stromagenesis during tumorigenesis: characterization of tumor-associated fibroblasts and stroma-derived 3D matrices. Methods Mol. Biol. 522: 275–305.
2. Beacham, D.A., M.D. Amatangelo, and E. Cukierman. 2007. Preparation of extracellular matrices produced by cultured and primary fibroblasts. Curr. Protoc. Cell Biol. Chapter 10: Unit 10.9.
3. Cukierman, E., R. Pankov, D.R. Stevens, and K.M. Yamada. 2001. Taking cell-matrix adhesions to the third dimension. Science. 294: 1708–12.

4. Doyle, A.D., M.L. Kutys, M.A. Conti, K. Matsumoto, R.S. Adelstein, et al. 2012. Micro-environmental control of cell migration--myosin IIA is required for efficient migration in fibrillar environments through control of cell adhesion dynamics. J. Cell Sci. 125: 2244–56.
5. Gentleman, E., A.N. Lay, D.A. Dickerson, E.A. Nauman, G.A. Livesay, et al. 2003. Mechanical characterization of collagen fibers and scaffolds for tissue engineering. Biomaterials. 24: 3805–3813.
6. Matthews, J., G. Wnek, D. Simpson, and G. Bowlin. 2002. Electrospinning of collagen nanofibers. Biomacromolecules. 3: 232–238.
7. Mogilner, A., and G. Oster. 2003. Force generation by actin polymerization II: the elastic ratchet and tethered filaments. Biophys. J. 84: 1591–605.
8. Johnson, K.L. 1985. Contact Mechanics. Aug 28, 19. New York: Cambridge University Press.
9. Goetz, J.G., S. Minguet, I. Navarro-Lérida, J.J. Lazcano, R. Samaniego, et al. 2011. Biomechanical remodeling of the microenvironment by stromal caveolin-1 favors tumor invasion and metastasis. Cell. 146: 148–63.
10. Cavalcanti-Adam, E.A., A. Micoulet, J. Blümmel, J. Auernheimer, H. Kessler, et al. 2006. Lateral spacing of integrin ligands influences cell spreading and focal adhesion assembly. Eur. J. Cell Biol. 85: 219–24.